MRPC noise limit of Alloy 690TT steam generator tube for detecting OD axial cracks and decreasing general corrosion rate

Hee-Sang Shim[1,*], Myung Sik Choi[1], Deok Hyun Lee[1], One Yoo[2], Do Haeng Hur[1]

Nuclear Materials Research Division, KAERI, 989-111 Daedeok-daero, Yuseong-gu, Daejeon 34057, Korea
KEPCO E&C Inc., 989-111 Daedeok-daero, Yuseong-gu, Daejeon 34057, Korea
[*]*Corresponding author: hshim@kaeri.re.kr*

1. Introduction

Alloy 600 steam generator (SG) tubes in pressurized water reactors (PWRs) have experienced various types of corrosion degradations such as pitting, intergranular attack, stress corrosion cracking. As a result of these problems, Alloy 600 has been replaced by thermally-treated (TT) Alloy 690 with a higher chromium concentration of 30%. Corrosion damages have not yet observed in Alloy 690TT since it was first used as a SG tube in 1989 [1]. Nevertheless, many researchers still believe that Alloy 690TT tubing material should be further studied for corrosion degradations in various environmental conditions, because its integrity has not been verified in long-term use.

It is difficult to keep the same surface state for the SG tubes used in the practical nuclear power plants because of the complex manufacturing process or careless installation [2,3]. The corrosion behavior of SG tubing is often associated with abnormal surface state [4]. Therefore, the surface preparation is very important for the corrosion control in nuclear power plants. The effect of surface state on corrosion degradations of Alloy 690TT tubing in the simulated nuclear power plant environment has been widely studied by many researchers [3, 5-7]. Zhang et al. found that the surface roughness and strain, which was leaded by surface finishing manner, could change the morphology and chemical composition of oxide films for Alloy 690TT [3]. Seo et al. reported that the corrosion rate of Alloy 690TT decreased with change in oxide morphology as its roughness became finer [5]. The surface state of Alloy 690TT also affects to its stress corrosion cracking (SCC) properties. The SCC-resistance of Alloy 690TT was reduced by cold-working and higher applied stress in Pb-containing caustic solution [6]. The macroscopic surface states such as drawing or pilgering marks, and circumferential thickness difference, which could be generated in manufacturing process, also affect to the general corrosion property of Alloy 690TT as well as its microscopic surface state. Shim et al. found that the general corrosion rate depended on the background noise amplitude of eddy current testing (ECT) signal measured using motorized rotating probe [8]. Herein, the noise level of ECT reflects inner surface states of SG tube. Noise signals arising from the tube degrade the probability of detection and sizing accuracy of defects [9]. Therefore, tube noise level is limited by specifying a minimum acceptance signal-to-noise ratio, which is measured using a bobbin coil probe [10]. However, the general corrosion behaviors was more closely correlated to the tube noise measured using a motorized rotating probe.

In this work, we investigated the relationship between crack detectability and the ECT noise measured using motorized rotating probe, and between general corrosion rate and the ECT noise. In addition, we would like to suggest the noise limit of Alloy 690TT tube in a point view of improvement of crack detectability and corrosion resistance of Alloy 690TT.

2. Experimental

2.1. Detection of OD axial cracks

Three Alloy 690TT SG tubes with an out diameter of 19.05 mm and a wall thickness of 1.1 mm were used to make artificial OD axial cracks. The tubes were manufactured by a pilgering process and had a different +point coil noise as summarized in Table 1. The axially-oriented cracks were made with 3 mm length using ultrafast laser scanner. The laser source is a commercial carbide laser system (Light Conversion Co.) providing linearly polarized laser pulses with a duration of 190 fs at a central wavelength of $\lambda = 1030$ nm and an repetition rate of 30 kHz. The focal length of scan lens was a 167 mm and scan speed was a 15 mm/s. The sixteen cracks were made on each tube at 10 mm intervals with increasing 10 scans. Then, the vapor generated by laser ablation was immediately removed by suction with argon blowing to prevent it fill up a crack.

The ECT signals were acquired using the Zetec MIZ-70 digital data acquisition system with a conventional 3-coil motorized rotating probe, which consists of two pancake coils and a plus point coil. The probe was inserted into the inside of the tube and is moved along the length of the tube at a pulling speed of 5.08 mm/s while being rotated at a constant rotating rate of 600 rpm. The signal from the axial throughwall electron discharge machining (EDM) notch of a 9.525 mm length was calibrated to be an amplitude of 20 V and a phase angle of 30 degrees at 300 kHz. The noise signals were measured at the region between an interest crack and next crack to reflect the local surface state of each tube. In addition, the +point coil signals were only compared to exclude the effect by thickness difference as a type of volumetric defect.

Table 1. +Point coil noise of Alloy 690TT SG tubes.

Tube ID	+Point coil noise (Volt)	
	V_{vmax}	V_{pp}
Tube A	0.05	0.06
Tube B	0.11	0.38
Tube C	0.17	0.60

Finally, the cracks were destructively examined to measure their actual length and depth using optical microscope (OM).

2.2. Investigation of general corrosion rate

Five Alloy 690TT SG tubes having different ECT noise value (as summarized in Table 2), which were used in practical nuclear power plants, with an out diameter of 19.05 mm and a wall thickness of 1.1 mm were used to investigate the general corrosion rate of Alloy 690TT tube in primary coolant condition. Corrosion test of Alloy 690TT tubes performed in a 4L Hastelloy C-276 autoclave with a circulation loop as shown in Fig. 1. A test solution simulating the primary water of PWRs was prepared by dissolving unclear-grade lithium hydroxide (LIOH) and boric acid (H_3BO_3) in deionized water. The test solution contained 2.0 ppm Li and 1,200 ppm B, and its pH was measured as approximately 6.3 at 25°C. The dissolved oxygen concentration and dissolved hydrogen concentration of the test solution were adjusted to less than 5 ppb and 35 cc(STP)H_2/kg·H_2O, respectively. The system pressure and temperature in the test autoclave were kept at 150 bar and 330°C, respectively. The corrosion test was conducted for 500, 1,000, and 3,000 h.

The corrosion rate of the tubes was evaluated by gravimetric analysis based on a descaling method. After the corrosion test, the oxidized corrosion specimens were descaled using a two-step alkaline permanganate (AP) and ammonium citrate (AC) process. The first step was conducted in an aqueous solution containing 1% $KMnO_4$ and 5% NaOH at 90°C for 30 min. The second step was performed in a 5% AC solution at 90°C for 30 min. After both steps, the weights of the specimens were measured using a five-place balance with an accuracy of 10 ug. In this way, the two-step descaling process was repeated on each specimen at least seven times. To correct the base metal losses from corrosion during the descaling process, the cumulative weight losses were reversely linear-extrapolated, according to the ASTM G1-03 standard [11]. Two corrosion specimens with an area of about 26.5 cm^2 were used to calculate the corrosion rates of the as-received and electropolished tubes. The morphology and microstructure of the surface oxide layer were investigated using SEM and X-ray diffraction.

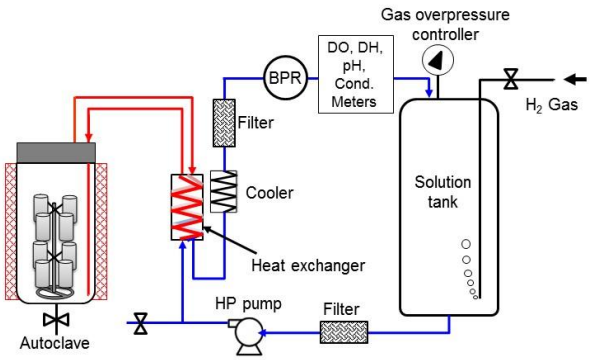

Fig. 1 Schematic of the primary water recirculating system used for the corrosion test.

Table 2. Vertical noise and peak-to-peak noise of +Point coil, and surface roughness for Alloy 690TT SG tubes. a) and b) indicate that the tube was manufactured by different process.

Tube ID	+Point coil noise (Volt)		Roughness (um)
	V_{vmax}	V_{pp}	
Tube D[a)]	0.05	0.06	0.20 ±0.008
Tube E[a)]	0.04	0.08	0.23 ±0.009
Tube F[a)]	0.09	0.16	0.24 ±0.010
Tube G[b)]	0.06	0.08	0.44 ±0.013
Tube H[b)]	0.04	0.05	0.50 ±0.011

3. Results and discussion

Three tubes were selected with different tube noise levels measured using the +point coil probe for fabricating the axial OD crack. The average noise level was measured as a V_{vmax} and a V_{pp}. Herein V_{vmax} and V_{pp} indicate a vertical maximum amplitude and a peak-to-peak amplitude of a tube noise signal, respectively. The relationship between V_{vmax} and V_{pp} can be explained by the following equation;

$$V_{pp} = \sqrt{V_{vmax}^2 + V_{hmax}^2} \qquad (1)$$

where, V_{hmax} is a horizontal maximum amplitude of the +point coil noise. In other words, V_{pp} is an amplitude between two points that are farthest apart vectorially in the Lissajous of +point coil noise signal, i.e., a vector sum of the vertical component and the horizontal component. The average V_{vmax} noise of each tube was 0.05 V(tube A), 0.11 V(tube B), and 0.17 V(tube C) as summarized in Table 1. In addition, V_{pp} value of each tube was 0.06 V(tube A), 0.38 V(tube B), and 0.60 V(tube C), respectively.

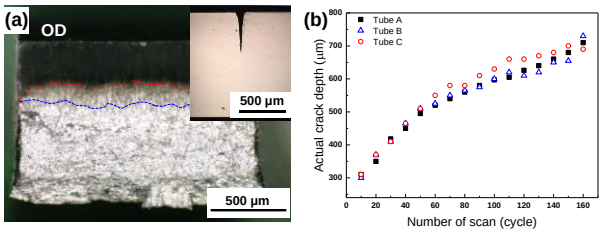

Fig. 2 (a) The destructive OM image of a 40% depth crack and (b) the relationship between the number of laser scan and the crack depth.

Fig. 2 shows the optical microscope (OM) image of longitudinal fracture surface for a 40% OD crack made using the ultrafast laser and the variation of crack depth as a function of laser scanning number. The color of fracture surface was distinguished by 3 zones such as blackish, brownish, and silvery regions as shown in Fig. 2(a). The circumferential cross-section of the crack displayed V-shape and the width of crack mouth was similar with about 100 μm for all laser-processed cracks. The width of the crack became gradually narrower to the inner diameter (ID) surface and was narrowed to about 5 μm at the crack tip as shown in the inset of Fig. 2(a). The crack depth was evaluated by about 40% of the wall thickness of tube but it seemed to be slightly different along the longitudinal direction of the crack. In addition, the crack depth measured in the cross-sectional image

seems to be agreed with the blue line including blackish and brownish regions. The crack depth increased gradually with increasing the number of laser scans and was similar value for the same treatment in all three tubes as shown in Fig. 2(b). The processability of the crack through laser scanning declined gradually as the crack depth became thicker.

Fig. 3 shows the relationship between crack depth and phase angle of +point coil signal measured at 300 kHz frequency. The solid line indicates the phase angle of ID and OD EDM notches with different depth. Then, the phase angle was 0 ~ 30 degrees for ID defect and 30 ~ 105 degrees for OD defect, when the signal of throughwall EDM notch (100% depth) is calibrated to be a phase angle of 30 degrees. It is obvious that all cracks produced on tube A, which has the lowest +point coil noise, is the OD defect because their phase angles are located in the range of 80 ~ 105 degrees. However, the phase angles of tube B and C, which showed higher +point coil noise, were investigated in the range of 4~85%. Herein, the cracks having the phase angle lower than 30 degrees can be discriminated as the ID crack because it is in the range of the phase angle of ID crack. This result might be because the phase angle of crack decreased due to interference of the signal with the horizontal noise.

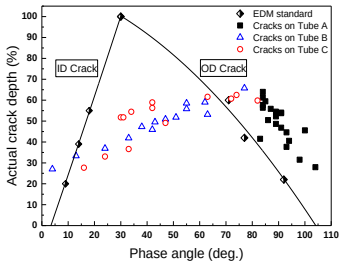

Fig. 3 The relationship between crack depth and phase angle; the solid line indicates the crack depth and phase angle of ID and OD EDM notches.

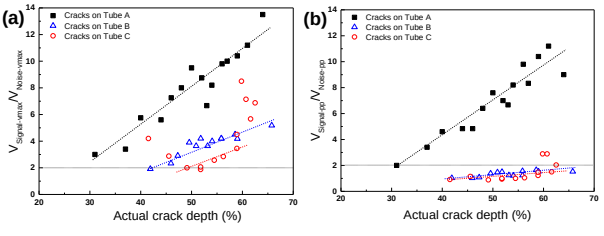

Fig. 4. The relationship between the signal-to-noise ratio and the depth of the crack with length of 3 mm; (a) $V_{Signal\text{-}vmax}/V_{Noise\text{-}vmax}$ and (b) $V_{Signal\text{-}pp}/V_{Noise\text{-}pp}$.

Fig. 4 shows the relationship between the signal-to-noise (S/N) ratio and the crack depth. All cracks fabricated on three tubes presented the value larger than 2 for the S/N ratio in a vertical component as shown in Fig. 4(a). However, the slope of the relationship between the $V_{Siganl\text{-}vmax}/V_{Noise\text{-}vmax}$ ratio and the crack depth became lower with increase of the +point coil noise. This indicates that the detection resolution of the crack in the vertical component decreases as the tube noise increases because the crack signal is interfered with the noise signal. The influence of the tube noise on the crack signal sizing was seen well in Fig. 4(b). The relationship of the $V_{Siganl\text{-}pp}$ with the $V_{Noise\text{-}pp}$, which is used to evaluate the size of crack, shows clear difference between tube A and other tubes. The $V_{Siganl\text{-}pp}/V_{Noise\text{-}pp}$ ratio also presented the value larger than 2 in tube A like as $V_{Siganl\text{-}vmax}/V_{Noise\text{-}vmax}$. However, the $V_{Siganl\text{-}pp}/V_{Noise\text{-}pp}$ ratio was about 1 for the cracks in tube B and C. In other words, this means that the sizing of the crack with 40~60% depth is difficult to be detected because the signal amplitude of the crack is equivalent to the noise amplitude. Both of $V_{Signal\text{-}vmax}$ and $V_{Signal\text{-}pp}$ of tube A were larger than 2 times comparing to the noise amplitude for all cracks, while tube B and C presented very low $V_{Signal\text{-}pp}/V_{Noise\text{-}pp}$ ratio of about 1, although its $V_{Siganl\text{-}vmax}/V_{Noise\text{-}vmax}$ was about 2. The size of cracks in tube B and C is difficult to be evaluated because the crack size is evaluated using the $V_{Signal\text{-}pp}$ value in industry and the S/N ratio become at least larger than 2 in a viewpoint of probability of detection (POD) of the examiner or in automatic evaluation program. Therefore, the +point noise level would be limited as low as possible to improve the detectability of the crack during in-service inspection (ISI).

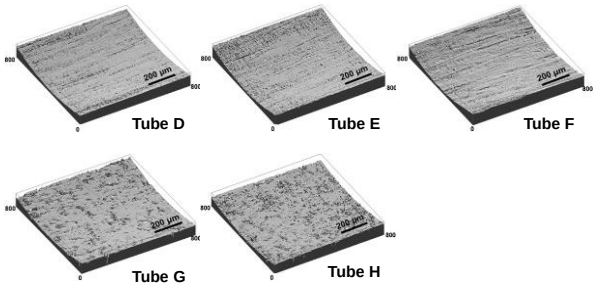

Fig. 5 Inner surface morphologies of five Alloy 690TT SG tubes.

Fig. 5 shows the three-dimensional surface topographies of the tubes D to H obtained using optical surface profiler. Herein, tube D~F were manufactured through pilgering process and tube G and H were made through drawing process. The pilgered tubes show a rough surface with long axial fissures, while the drawn tubes show gulling marks over whole surface. These might depend on processing tools and forming mechanism.

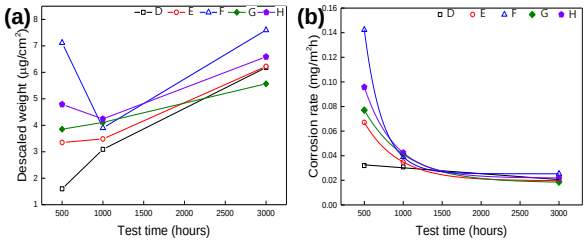

Fig. 6 (a) Descaled weight and (b) corrosion rate of the tubes converted from the descale weight.

Fig. 6(a) shows the weight of oxide films formed on the tubes through chemical descaling process. In addition, Fig. 6(b) reveals the corrosion rate calculated from the decaled oxide weight values of the tubes. The descaled weight increases and corrosion rate decreases as the test time increases. However, the trend in descaled weight

and corrosion rate could not be recognized for manufacturing methods and ECT noises.

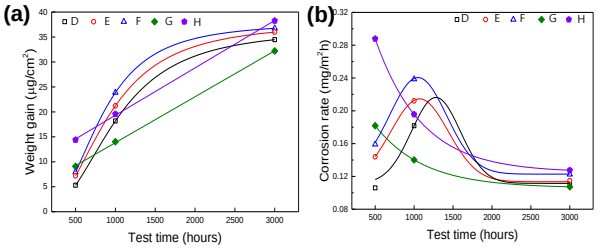

Fig. 7 (a) Weight gain and (b) corrosion rate of the tubes converted from the weight gain.

Fig. 7 shows the simple weight gain measured from the corroded specimens and the corrosion rate calculated from the weight gain values. There is significant difference for manufacturing processes of the tubes. The pilgered tubes show exponential increase in weight gain values, while the drawn tubes show proportional increase as the test time increases. Furthermore, the pilgered tubes display the highest corrosion rate for 1,000 h corroded specimens, while the drawn tubes show exponential decrease as the test time increases. These results indicate that the corrosion behavior can be affected the manufacturing method of the SG tube. Furthermore, the corrosion rate decreases on the tubes with lower ECT noise value without manufacturing method of the tubes.

4. Conclusions

In this work, we fabricated the artificial cracks on Alloy 690TT SG tube using ultrafast laser scanning method to evaluate the influence of +point coil noise on the detectability of the axial OD crack. Tube A with low +point noise is easy to detect and to evaluate the size of the crack. However, tube B and C with high noise, which is equivalent to the amplitude of flaw signal, is difficult to evaluate the size of the cracks of 40~60% depth. Therefore, the +point coil noise would be limited from the manufacturing step to improve the detectability of the flaws during ISI as low as possible. In addition, the general corrosion rate of Alloy 690TT tubes shows lower value as the +point coil noise and it is affected by manufacturing method. Therefore, considering both detectability of the corrosion damage and the corrosion rate in PWR primary water, the ECT noise of Alloy 690TT tubes would be controlled to lower value as soon as possible.

Acknowledgments

This work was supported by the National Research Foundation of Korea (NRF) grant funded by the Korea government (2017M2A8A4015159).

REFERENCES

[1] R. W. Steahle, J. A. Gorman, Quantitative assessment of submodes of stress corrosion cracking on the secondary side of steam generator tubing in pressurized water reactors: Part 1. Corrosion Vol. 59, pp. 931-994, 2003.
[2] H. Abe, M. Furugen, Method of evaluating workability in cold pilgering of zirconium alloy tube, Mater. Trans. Vol. 52 pp.1200–1205, 2010.
[3] Z. Zhang, J. Wang, E.-H. Han, W. Ke, Characterization of Diffeent Surface States and Its Effects on the Oxidation Behaviors of Alloy 690TT, J. Mater. Sci. Technol., Vol. 28, pp. 353-361, 2012.
[4] F. J. Meng, J. Q. Wang, E.-H. Han, W. Ke, Effects of scratching on corrosion and stress corrosion cracking of Alloy 690TT at 58ºC and 330ºC, Corrosion Science Vol. 51, pp. 2761-2769, 2009.
[5] M.J. Seo, H.-S. Shim, K.M. Kim, S.-I. Hong, D.H. Hur, Influence of surface roughness on the corrosion behavior of Alloy 690TT in PWR primary water, Nucl. Eng. Des., Vol. 280, pp. 62-68, 2014.
[6] Z. Zhang, J. Wang, E.-H. Han, W. Ke, Effects of Surface State and Applied Stress Corrosion Cracking of Alloy 690TT in Lea-containing Caustic Solution, J. Mater. Sci. Technol., Vol. 28, pp. 785-792, 2012.
[7] Materials Reliability Program: Resistance to Primary Water Stress Corrosion Cracking of alloys 690, 52 and 152, in Pressurized Water Reactors (MRP-111), TR-1009801, EPRI, Palo Alto, CA, 2004.
[8] H.-S. Shim, M. S. Choi, D. H. Lee, D. H. Hur, A prediction method for the general corrosion behavior of Alloy 690 steam generator tube using eddy current testing, Nucl. Eng. Des., Vol. 297, pp. 26-31, 2016.
[9] Measuring and Monitoring Noise in Steam Generator Tubing Eddy-Current Dat for Tube Integrity Applications, TR-1016554, EPRI, Palo Alto, CA, 2008.
[10] Advanced Nuclear Technology: Alloy 690 Steam Generator Tubing Specification Sourcebook, TR-3002009412, EPRI, Palo Alto, CA, 2016.
[11] Standard practice for preparing, cleaning, and evaluating corrosion test specimens, ASTM G1-03, ASTM, 2011.